Electrochemistry of Fischer alkoxycarbene complexes of chromium: The use of Density Functional Theory to predict and understand oxidation and reduction potentials

Marilé Landman[a], Renyuan Lui[b], Petrus H. van Rooyen[a] and Jeanet Conradie[b]**

a Department of Chemistry, University of Pretoria, Private Bag X20, Hatfield, 0028, South Africa. Tel: 27-12-4202527 Fax: 27-12-4204687

b Department of Chemistry, PO Box 339, University of the Free State, Bloemfontein, 9300, South Africa. Tel: 27-51-4012194, Fax: 27-51-4446384

Contact author details:

Name: Marilé Landman Tel: ++27-12-4202527 Fax: ++27-12-4204687, email: *marile.landman@up.ac.za*

Name: Jeanet Conradie, Tel: ++27-51-4012194, Fax: ++27-51-4446384, email: *conradj@ufs.ac.za*

Abstract

The electrochemical behaviour of a series of Fischer ethoxycarbene complexes of the type $[(CO)_5Cr=C(OEt)R]$ with R = 2-thienyl (**1**), 2-furyl (**2**), 2-(N-methylpyrrolyl) (**3**), N-methyl-2-(2'-thienyl)pyrrole) (**4**) and 2,2'-thienylfuran (**5**), is investigated by means of cyclic voltammetry. Results show that the first one electron reduction process is sensitive to the energy, shape and distribution of the LUMO orbital, leading to a linear relationship between the formal reduction potential and the LUMO energy: $E^{0'}(C_{carbene}) = -0.70\ E_{LUMO} - 3.44$ ($R^2 = 1.00$) which is valid over a large potential

range. The dimeric heteroarene substituents of **4** and **5** lead to enhanced stabilization of the reduced complexes **4** and **5**, making another one electron reduction possible. The formal reduction potential, $E^{0'}$(Cr) of the first oxidation process of **1**-**5** lays within a narrow potential range of 0.43 to 0.50 V *vs*. Fc/Fc^{+}, is Cr-based and is mainly sensitive to the electrophilic character of the heteroarene ring directly attached to the carbene carbon.

Keywords

Fischer alkoxycarbene Cr-complexes, Electrochemistry, DFT calculations

1 Introduction

Fischer carbene complexes are characterized by the presence of a formal double bond, $M=CR_2$, between the central metal atom M and the carbene ligand, CR_2. The carbene carbon atom is electrophilic in nature [1]. Stabilization by electron-donating substituents, such as heteroatoms and heteroarene rings, occurs through electron density transfer from the electron-rich substituent into the empty p-orbital on the carbene carbon atom [2,3]. Due to the application of Fischer carbene complexes to organic synthesis [4,5] and catalysis [6], understanding the reactivity of the complexes becomes important.

The electrochemical properties of chromium aminocarbenes have been well studied [7,8,9,10], while electrochemical properties of only few examples of chromium ethoxycarbene complexes, $[(CO)_5Cr=C(OEt)R]$ (with R = thienyl or ferrocenyl or furyl), have been published to date [11]. In a recent electrochemical study, a series of aminocarbene complexes of chromium(0) containing five-membered heteroaromatic rings, was investigated [10]. Furyl, thienyl or N-methylpyrrolyl substituents on the carbene carbon were attached either at the 2- or 3-position of the heteroarene ring. Although it was concluded that neither changing the heterocycle, nor changing the position of attachment significantly influenced the oxidation behaviour, the reduction behaviour was much more sensitive to the nature of the heteroarene and the position

of attachment. Attachment at position 2 made reduction much easier because of stabilization of the reduction intermediate.

Heteroarene five-membered rings can be linked at the 2'-position to form stable dimers. Coordination to metal-containing substituents can facilitate charge transfer or electron delocalization in the molecule [12]. The π-conjugation through the molecule is evident from the planarity of the dimeric heteroarene substituent. We were interested in determining the influence of a dimeric heteroarene five-membered ring system on the reactivity of chromium alkoxycarbene complexes. In this article the electrochemical behaviour of mononuclear ethoxycarbene complexes (**1**-**5**) with electron-rich heteroaromatic substituents is reported (Figure 1). Structural features of the complexes were studied in the solid state by crystal structure determinations. A computational chemistry study provides a better understanding of the oxidation and reduction processes. In order to direct future synthesis of new ethoxycarbene complexes, relationships between density functional theory (DFT) energies and experimentally measured formal electrode potentials are presented.

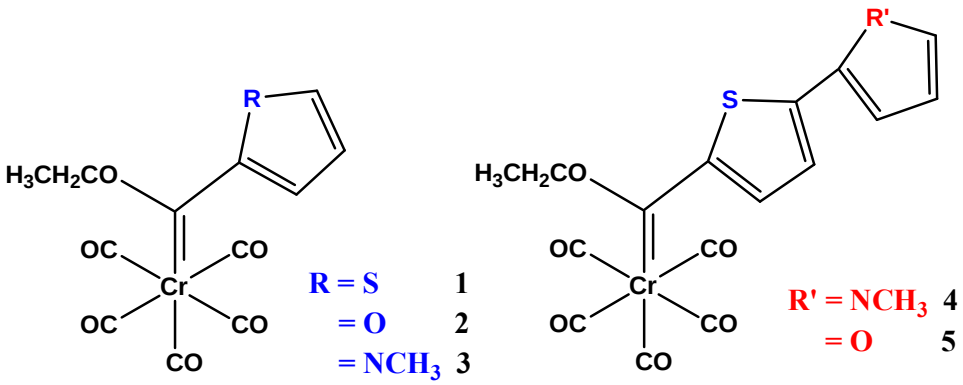

Figure 1: Cr ethoxycarbene complexes of this study

2 Experimental

2.1 General

All syntheses were carried out using standard Schlenk techniques under an inert atmosphere of nitrogen or argon gas [13]. Solvents were dried prior to use. Nuclear

magnetic resonance spectra were recorded on a Brüker AC-300 spectrometer in $CDCl_3$ as solvent. ^1H NMR spectra were recorded at 300.135 MHz and ^{13}C NMR spectra at 75.469 MHz with the solvent signal as reference. Infrared spectra were recorded as KBr pellets on a PerkinElmer Spectrum RX FT-IR instrument and the vibrational bands of the carbonyl ligands in the region 1700-2200 cm^{-1} reported. Chromatographic separations and purification were performed using nitrogen gas saturated kieselgel (0.063-0.200 mm). Thiophene was purified as described in literature, prior to use [14]. Triethyloxonium tetrafluoroborate was prepared according to a literature procedure [15]. The following dimeric heteroarene precursors and carbene complexes were synthesized according to known literature methods: 2,2'-Thienylfuran (**A**) [38] and N-methyl-2-(2'-thienyl)pyrrole (**B**) [38], $[Cr(CO)_5C(OEt)(2\text{-thienyl})]$ (**1**) [43], $[Cr(CO)_5C(OEt)(2\text{-furyl})]$ (**2**) [43], $[Cr(CO)_5C(OEt)(2\text{-(N-methylpyrrolyl)})]$ (**3**) [16] and $[Cr(CO)_5C(OEt)$(N-methyl-2-(2'-thienyl)pyrrole)] (**4**) [38]. Characterization data of **1**-**4** were in agreement with these literature reports.

2.2 Synthesis

$[Cr(CO)_5C(OEt)$2,2'-thienylfuran] (**5**) [38]

2,2′-Thienylfuran (0.38 g, 2.5 mmol) was dissolved in tetrahydrofuran (THF) (30 ml) and the solution cooled to -20 °C. 1.7 ml (2.8 mmol) of a 1.6 M solution of *n*-BuLi in hexane was added and the reaction mixture stirred for 30 minutes. The temperature of the cold bath was lowered to -40 °C and $Cr(CO)_6$ (0.67 g, 2.5 mmol) was added in small portions. An immediate colour change was observed to dark brown. The mixture was stirred for a further 30 minutes after which time the cold bath was removed and the brown reaction mixture stirred at room temperature for 1h. The solvent was removed *in vacuo*. The brown residue was dissolve in dichloromethane and the reaction mixture cooled to -20 °C. 0.10 g (2.5 mmol) Et_3OBF_4, dissolved in 15 ml of dichloromethane (DCM), was added. The reaction mixture was stirred in the cold for 30 min and for a further 30 min at room temperature. The solvent was removed *in vacuo*. The residue was purified by column chromatography. The target complex was eluted from the column using hexane.

Complex **5:** Yield = 76%; Red-orange colour. ^{1}H NMR (δ(ppm), J(Hz)): H8 8.18 (d), 4.2; H9 7.34 (d), 4.2; H12 6.78 (d), 3.7; H13 6.51 (dd), 3.7, 1.9; H14 7.50 (d) 1.9; H15 5.13 (q), 7.2; H15 1.65 (t), 7.2. ^{13}C NMR (δ(ppm): C7 315.2 Cr(**C**O)$_5$ 223.8 217.2 C8 142.7, C9 124.0, C12 109.6, C13 112.8, C14 143.9, C15 76.3, C16 15.2. IR (cm^{-1}, KBr): 2057 m (A"$_1$), 1986 vw (B), 1960 s (A'$_1$), 1947 vs (E).

Table 1: Crystallographic data for 4 and 5

	4	**5**
Chemical formula	$C_{17}H_{13}CrNO_6S$	$C_{16}H_{10}CrO_7S$
MW (g mol^{-1})	411.34	398.30
Crystal system	Monoclinic	Monoclinic
Space group	P 2_1/c	P 2_1/c
a (nm)	a = 0.73650(4)	a = 1.65695(7)
b (nm)	b = 1.26640(7)	b = 0.67139(3)
c (nm)	c = 1.91042(10)	c = 1.69497(8)
α (º)	α = 90	α = 90
β (º)	β = 95.883(2)	β = 117.888(1)
γ (º)	γ = 90	γ = 90
Volume (nm^3)	1.7725(2)	1.6666(1)
Z	4	4
d_{calcd} (Mg m^{-3})	1.541	1.587
μ (mm^{-1})	0.797	0.847
Crystal size (mm^3)	0.101 x 0.112 x 0.196	0.074 x 0.078 x 0.366
θ range (º)	2.680 to 26.371	2.406 to 26.369
Index range	$-9 \le h \le 9$, $-15 \le k \le 15$, $-23 \le l \le 23$	$-20 \le h \le 20$, $-8 \le k \le 8$ $-21 \le l \le 21$
Reflections collected	61025	45988
Independent reflections	3624 [R(int) = 0.0305]	3416 [R(int) = 0.0499]
Final R indices [I>2σ(I)]	R1 = 0.0332, wR2 = 0.0919	R1 = 0.0443, wR2 = 0.0986
R indices (all data)	R1 = 0.0357, wR2 = 0.0936	R1 = 0.0584, wR2 = 0.1047

2.3 Crystallography

Data for a red crystal of **4** and an orange crystal of **5** were collected at 150 K on a Bruker D8 Venture kappa geometry diffractometer, with duo Iμs sources, a Photon

100 CMOS detector and APEX II [17] control software using Quazar multi-layer optics monochromated, Mo-*K*α radiation by means of a combination of ϕ and ω scans. Data reduction was performed using SAINT+ [17] and the intensities were corrected for absorption using SADABS [17]. The structure was solved by intrinsic phasing using SHELXTS [18] and refined by full-matrix least squares using SHELXTL [18] and SHELXL-2012 [18]. In the structure refinement all hydrogen atoms were added in calculated positions and treated as riding on the atom to which they are attached. All non-hydrogen atoms were refined with anisotropic displacement parameters, all isotropic displacement parameters for hydrogen atoms were calculated as X × Ueq of the atom to which they are attached, X = 1.5 for the methyl hydrogens and 1.2 for all other hydrogens. The crystallographic data for **4** and **5** are given in Table 1.

2.4 Cyclic Voltammetry

Cyclic voltammogram (CV) and linear sweep voltammogram (LSV) measurements were performed on 0.0005(0.00005) mol dm^{-3} compound solutions in dry acetonitrile containing 0.1 mol dm^{-3} tetra-*n*-butylammonium hexafluorophosphate, ($[^n(Bu_4)N][PF_6]$), as supporting electrolyte and under a blanket of purified argon at 21 °C utilizing a Princeton Applied Research PARSTAT 2273 voltammograph running PowerSuite (Version 2.58). A three-electrode cell, with a glassy carbon (surface area 7.07 x 10^{-6} m^2) working electrode, Pt auxiliary electrode and a Ag/Ag^+ (0.010 mol dm^{-3} $AgNO_3$ in CH_3CN) reference electrode [19] mounted on a Luggin capillary, was used [20,21]. All temperatures were kept constant to within 1 °C. Scan rates were 0.050 – 5.000 V s^{-1}. Successive experiments under the same experimental conditions showed that all oxidation and formal reduction potentials were reproducible within 0.010 V. All cited potentials were referenced against the Fc/Fc^+ couple as suggested by IUPAC [22]. Ferrocene exhibited a formal reduction potential $E°'$ = 0.079 V *vs.* Ag/Ag^+, a peak separation $\Delta E_p = E_{pa} - E_{pc}$ = 0.069 V and i_{pc}/i_{pa} = 1.00 under our experimental conditions. E_{pa} (E_{pc}) = anodic (cathodic) peak potential and i_{pa} (i_{pc}) = anodic (cathodic) peak current. $E°'$ (Fc/Fc^+) = 0.66(5) V (0.77(5) V) *vs.* SHE in $[^n(Bu_4)N][PF_6]/CH_3CN$ (DCM) [23].

2.5 DFT calculations

All density functional theory (DFT) calculations were performed with the hybrid functional B3LYP [24,25] as implemented in the Gaussian 09 program package [26]. Geometries were optimized in gas phase with the triple-ζ basis set 6-311G(d,p) on all atoms except chromium, where LANL2DZ was used (corresponding to the Los Alamos Effective Core Potential plus DZ [27,28,29,30]). Solvation effects were computed by performing full geometry optimizations with the IEFPCM model, using either acetonitrile (ε = 37.5) or dichloromethane (ε = 8.9) as solvent.

3 Results and Discussion

3.1 Synthesis of carbene complexes 1-5

Several catalytic methods for the preparation of dimeric heterocyclic compounds have been published in literature [31,32,33,34,35,36,37]. The dimeric heteroarene precursors used in this study were synthesized according to known literature methods [38]. 2,2'-Thienylfuran (**A**) was synthesized from 2-tributylstannylfuran [39] and 2-bromothiophene *via* the Stille reaction. A Negishi cross-coupling reaction [40] was used to prepare N-methyl-2-(2'-thienyl)pyrrole (**B**) from 2-(N-methylpyrrolyl)zinc chloride and 2-bromothiophene.

The α-monodeprotonation of heteroarene rings is more readily achieved for thiophene and furan than for N-methylpyrrole. The position of lithiation for dimeric heteroarene compounds containing two different rings can be controlled by varying the reaction conditions. Furan will be α-lithiated by preference in hexane in a competitive reaction with thiophene for an insufficient quantity of *n*-BuLi [41]. By contrast, thiophene is deprotonated more rapidly than furan at low temperatures in tetrahydrofuran, reaction conditions that favour the ionisation of the C–Li bond [42]. Thermal conditions are necessary to deprotonate the α-position of N-methyl pyrrole. Both **A** and **B** were deprotonated in THF at -20 °C, mono-lithiating the α-position of the thiophene ring in each case.

Classic Fischer methodology was employed to synthesise the chromium pentacarbonyl alkoxycarbene complexes [$(CO)_5CrC(OEt)R$]; R = 2-thienyl (**1**) [43], 2-furyl (**2**) [43], 2-(N-methylpyrrolyl) (**3**) [16], N-methyl-2-(2'-thienyl)pyrrole (**4**) [38] and 2,2'-thienylfuran (**5**) [38] (Scheme 1). After deprotonation of the heteroarene ring, chromium hexacarbonyl was added in a single portion at -40 °C and the reaction followed a nucleophilic mechanism in which an electrophilic metal carbonyl carbon is attacked by the newly formed nucleophilic, deprotonated heteroarene ring. The chromium metal acylate is formed as product. The solvent was removed under vacuum and the resulting residue dissolved in dichloromethane. Alkylation with triethyl oxonium salt at -20 °C resulted in formation of the desired monocarbene complex. Purification was done using silica gel chromatography with hexane and dichloromethane as eluents. Characterization data of **1-4** were compared with literature to confirm composition.

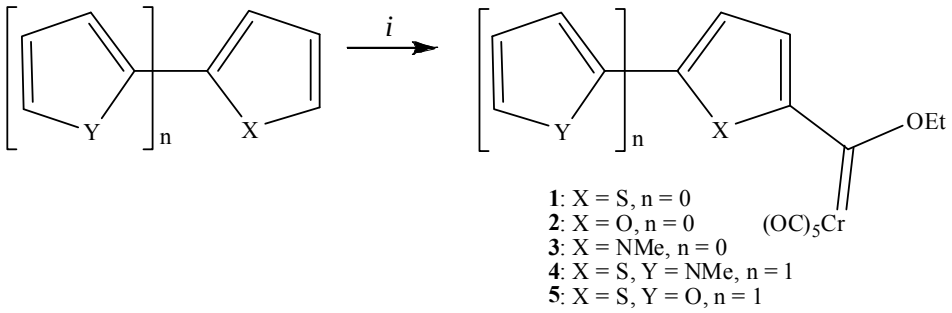

Scheme 1: Synthetic methodology for the chromium(0) carbene complexes (1)-(5) Reagents and conditions: (i) a. 1.1 eq. n-BuLi, thf, -20 °C; b. 1 eq. $Cr(CO)_6$, thf, -40 °C; c. Et_3OBF_4, CH_2Cl_2, -20 °C.

3.2 Single crystal X-ray structures of 4 and 5

The perspective drawings of **4** and **5** are shown in Figure 2 and Figure 3. Structural parameters of importance are summarized in Table 2. Of interest is that the Cr1-carbene distance of 0.2066(3) nm in **5** is significantly shorter that the distance of 0.2084(2) nm observed in **4**. The mean Cr1-C bond distances for carbonyls *cis* to the carbene bond are the same for both compounds. However, the difference between the longest and shortest Cr1-C(*cis*) bond in **5** is 0.0032 nm, while only 0.0013 nm in **4**. The conformations of both structures are very similar in that C1, O1, Cr1, C6, O6,

C15 and the non-hydrogen atoms of the heteroarene rings are all planar. The main difference in the conformation of the two compounds is that the C16 methyl group of **5** is not in this plane, indicated by the C6-O6-C15-C16 dihedral angle of 38.9(3) °. This may be a result of packing forces in the solid state as there seems to be no other steric or electronic reasons for this deviation from planarity. There were no other unusual aspects observed in the crystallographic packing of these molecules.

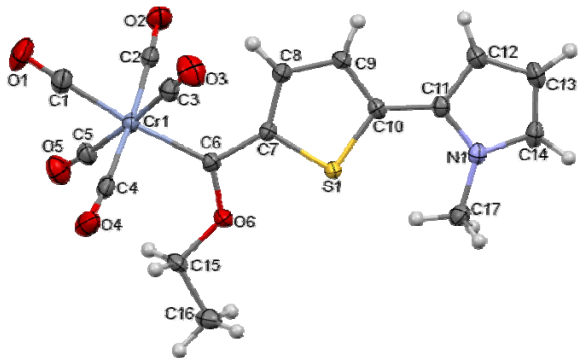

Figure 2: An Ortep drawing of the molecular structure of 4 showing the atom numbering scheme. ADPs are shown at the 50% probability level.

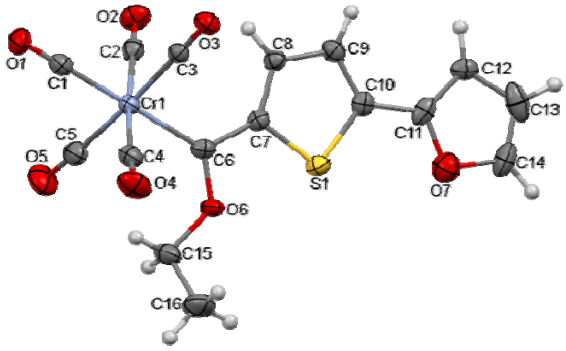

Figure 3: An Ortep drawing of the molecular structure of 5 showing the atom numbering scheme. ADPs are shown at the 50% probability level.

Table 2: Selected bond lengths (nm) and angles (°) of 4 and 5.

Bond length (nm)	**4**	**5**
Cr-C6$_{carbene}$	0.2084(2)	0.2066(3)
Cr1-C$_{(carbonyl)}$[a]	0.1902(2)	0.1902(3)
Cr1-C1[b]	0.1884(2)	0.1885(3)
C6-O6	0.1333(2)	0.1332(3)
C6-C7	0.1442(2)	0.1442 (4)
Bond angle (°)		
C1-Cr1-C6	174.7(1)	179.2(1)
Cr1-C6-O6	129.6(1)	128.5 (2)
Cr1-C6-C7	124.3(1)	125.5 (2)
O6-C6-C7	106.1(2)	106.0(2)
Torsion angle (°)		
C6-O6-C15-C16	2.1(2)	38.9(3)
O6-C6-C7-S1	0.9(3)	0.9(3)
S1-C10-C11-O7/N1	0.2(3)	1.1(4)

[a] Mean Cr1-C bond distance for carbonyls *cis* to the carbene ligand
[b] Cr1-C bond distance for carbonyl *trans* to the carbene ligand

3.3 Electrochemical and DFT study

The Cr ethoxycarbene complexes of this study (Figure 1) represent molecules with two redox active centres: the Cr metal and the carbene as "non-innocent" ligand [44,45]. Examples of the cyclic voltammograms (CVs) of **1**-**5**, obtained in dry, oxygen-free CH_3CN utilizing 0.1 mol dm^{-3} [$^n(Bu_4)N][PF_6$] as supporting electrolyte, are given in Figure 4 and the data summarized in Table 3. Three main redox processes are observed in the solvent window: one reduction process ascribed to the reduction of the carbene carbon atom and two oxidation processes: the oxidation of the Cr(0) metal centre to Cr(I) and the oxidation of electrochemically generated Cr(I) species to either Cr(II) or $(CO)_5$Cr(I)=C(OEt)R(+).

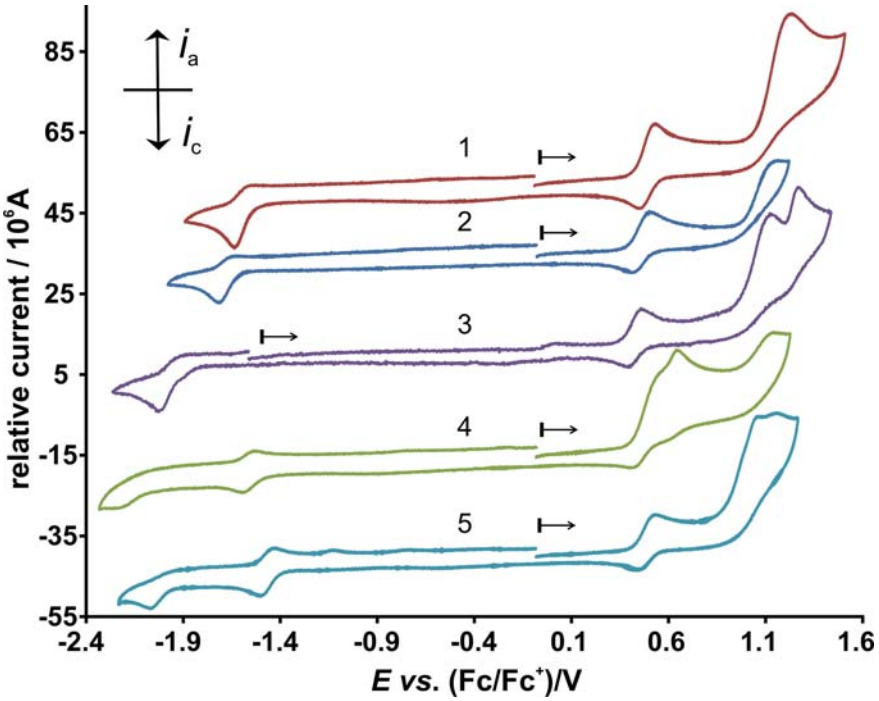

Figure 4: Cyclic voltammograms of 0.0005 mol dm^{-3} solutions of 1-5 in CH_3CN / 0.1 mol dm^{-3} [^{n}(Bu_4)N][PF_6] on a glassy carbon-working electrode at a scan rate of 0.100 V s^{-1}.

Figure 5 shows the cyclic voltammogram (CV) and the linear sweep voltammetry (LSV) of a 0.0005 mol dm^{-3} solution of **1** as well as the CV and LSV of 0.0005 mol dm^{-3} of ferrocene. Under the experimental conditions used, $\Delta E_p = E_{pa} - E_{pc} = 0.069$ V and $i_{pc}/i_{pa} = 1.00$ for ferrocene. The experimental peak separation of 0.069 V is larger than the Nernstian value of 0.059 V (for a one electron process) due to uncompensated ohmic drops in the cell. Consequently, for this study, ΔE_p values up to 0.090 V will be considered as indicative of an electrochemically reversible couple. From the Randles-Sevcik equation, $i_p = (2.69X10^5)n^{1.5}AD^{0.5}C\nu^{0.5}$, i_p = peak current (A), n being the number of exchanged electrons, A the electrode area (cm^2), ν scan rate (V s^{-1}), D the diffusion coefficient (cm^2 s^{-1}) and C the bulk concentration (mol cm^{-3}) of the electroactive species [46]), it follows that the diffusion coefficient $D^{0.5} \propto \frac{i_p}{\nu^{0.5}}$ if the concentration and electrode area is constant. For 0.0005 mol dm^{-3} of ferrocene under the experimental conditions used, $\frac{i_p}{\nu^{0.5}}$ = 40.14 (10^6A mV$^{-1/2}$s$^{+1/2}$). This is exactly the same value obtained for the oxidation of complex **1**, see Figure 7

(b). This implies that the diffusion coefficient of complex **1** and ferrocene is the same in CH^3CN as solvent. In this case the peak currents and LSV of the same concentration of complex **1** and ferrocene can be compared. Comparing the LSV of the two oxidation processes observed for **1** with that of ferrocene, it is concluded that each oxidation process represents a one electron oxidation only. The anodic current of the second irreversible oxidation process of **1** leads to adsorption and decomposition, implying that the peak current value is not reliable. Comparing peak currents and LSV data, a one electron reduction process is thus found for the chromium ethoxycarbene complexes of this study, reducing the neutral carbene complex to a radical anion species. A one electron reduction process was also found for the chromium ethoxycarbene and aminocarbene complexes in literature in DCM as solvent [11], while a series of chromium aminocarbene complexes showed a two electron reduction process utilizing the same solvent/electrolyte system as this study but a hanging mercury drop electrode (HMDE) [7,8,9,10] for CV measurements.

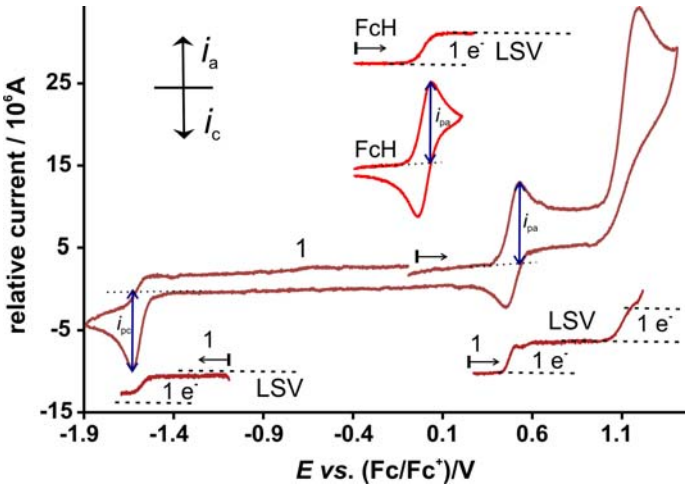

Figure 5: Cyclic voltammograms (CV at 0.050 V s^{-1}) and linear sweep voltammetry (LSV at 0.001 V s^{-1}) of 0.0005 mol dm^{-3} solutions of 1 (brown) and ferrocene (FcH, red) in CH_3CN / 0.1 mol dm^{-3} [$^n(Bu_4)N][PF_6]$ on a glassy carbon-working electrode.

Figure 7 shows the CV's at different scan rates for **1** and **5**, as well as graphs of peak currents versus $\nu^{0.5}$. The ratio of the slopes for complex **1** to that of complex **5** is *c.a.* 0.65, implying that the diffusion coefficient D of **5** is *c.a.* $(0.65)^{1/2}$ = 0.8 of that of complex **1**. It is expected that D of complex **5** will be lower than that of complex **1**

given the Stokes - Einstein relation, $D = kT/6\pi\eta r$, for diffusion of spherical particles through a liquid, and the increase in molecular size of **5** due to the additional aryl ring. (η is viscosity and r is the radius of the spherical particle).

3.3.1 $C_{carbene}$ reduction

Reduction of a complex involves the addition of an electron to the lowest occupied molecular orbital (LUMO) of the complex. Therefore the character of the LUMO of a complex should indicate where the reduction process will occur, while the singly occupied molecular orbital (SOMO) of the reduced complex will show where the first reduction took place. Complexes **1-5** of this study are all diamagnetic, implying that the reduced species will be paramagnetic with spin = ½ (one unpaired electron in the SOMO of the reduced species.). A visualization of this unpaired electron spin density will also give the same information; the location of the added unpaired electron. Figure 6 shows (a) the LUMOs of the neutral **1-5**, (b) the SOMOs of the reduced (charge q = -1) **1-5** and (c) the spin density of the reduced radical anions of **1-5**. All the diagrams in Figure 6 provide the same information, namely that the reduction involves the electrophilic carbene carbon and that the added electron density is delocalized over the heteroarene five-membered rings. The reduced species, the radical anion, is thus stabilized by distribution of the charge over the carbene carbon and the five-membered rings. It is clear that the reduction centre is mainly localized on the carbene ligand. This interpretation is in agreement with literature [11] and ESR experiments on $[(CO)_5Cr{=}C(OEt)Ph]$, where addition of an electron forms a carbon-centred radical with the odd electron localized on the carbene ligand [47].

The extended dimeric heteroarene five-membered ring systems of **4** and **5** lead to enhanced stabilization of the radical anion to such an extent that the reduction process is electrochemically reversible at all scan rates 0.050 – 5.000 V s^{-1}. At low scan rates, the reduction process of **1-3** is irreversible, *i.e.* no re-oxidation peak is observed. However, at higher scan rates, the peak current of the backward scan of the reduction process of **1-3** becomes more enhanced. At a scan rate of 0.3 V s^{-1}, the peak current separation of **1-3**, ΔE, becomes 0.07 – 0.08 V. This implies that the radical anion is

stabilized long enough on the timescale of the CV to be oxidized back to the neutral complex. See Figure 7(a) for the CV of **1** at different scan rates.

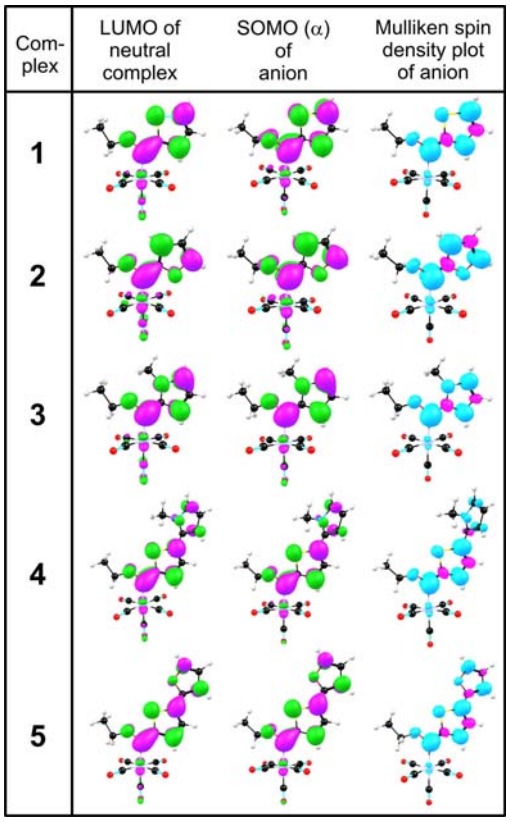

Figure 6: Presentation of (a) the LUMO of the neutral complexes 1-5, (b) the SOMO of the reduced (q = -1) complexes 1-5 and (c) the spin density of the reduced radical anion of complexes 1-5. The MO and spin density plots use a contour of 40 and 4 e/nm^3 respectively.

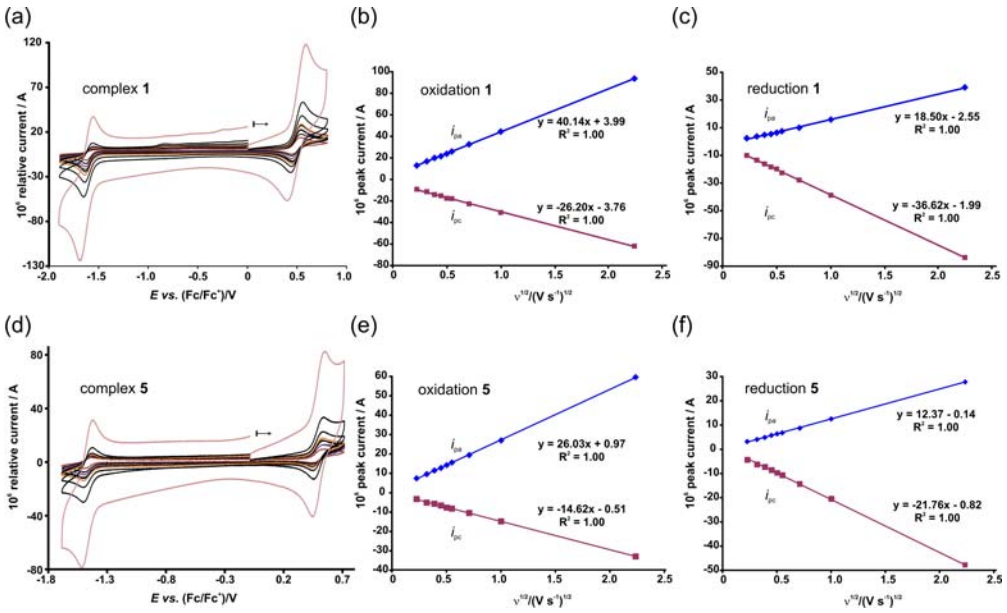

Figure 7: Cyclic voltammograms of 0.0005 mol dm^{-3} of (a) 1 and (d) 5, at scan rates of 0.050 – 5.000 V s^{-1}. Measurements were performed in 0.1 M [^{n}(Bu$_4$)N][PF$_6$]/CH$_3$CN on a glassy carbon working electrode at 20 °C. Scans are initiated in the positive direction, as indicated by the arrow. Dependence of peak current on (sweep rate)$^{1/2}$ for the Cr$^{0/I}$ oxidation process of (b) 1 and (e) 5, and for the C$_{carbene}$ reduction process of (c) 1 and (f) 5.

For **4** and **5** another reduction process, 0.5 – 0.6 V more negative than the first reduction process is observed. This second reduction is possible due to the stability of the radical anion of the first reduction process. The second reduction is, however, electrochemically and chemically irreversible. The lowest singly unoccupied molecular orbital (SUMO) of the radical anion of the first reduction process (q = -1) indicates that the second reduction also predominantly involves the carbene carbon atom and the heteroarene ring system, see Figure 8(a). The second reduction can lead to a diamagnetic complex with no unpaired electrons (S = 0, a singlet) or a paramagnetic complex with two unpaired electrons (S = 1, a triplet). DFT calculations show that the singlet is more than 1 eV more stable than the triplet. The highest occupied molecular orbital (HOMO) of the doubly reduced complex, Figure 8 (b), shows that the second reduction is also carbene carbon atom based with the electrons delocalized over the dimeric aromatic ligand.

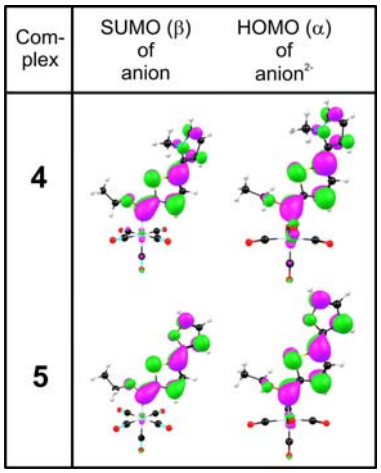

Figure 8: Presentation of the (a) SUMO of the reduced (q = -1, S = 1/2) and (b) HOMO of the doubly reduced (q = -2, S = 0) complexes 4 and 5. The MO plots use a contour of 40 e/nm^3.

3.3.2 Cr(0)-Cr(I) oxidation

Oxidation of a complex involves the removal of an electron from the HOMO of the complex. The character of the HOMO of the neutral complex will thus show where the oxidation will take place; the SUMO of the oxidized species will give an indication of where the electron had been removed. The localization of the unpaired free electron of the oxidized species, can be visualized by a spin-density of the oxidized species (q = +1, spin = ½). Figure 9 gives (a) the HOMO of the neutral **1**, (b)

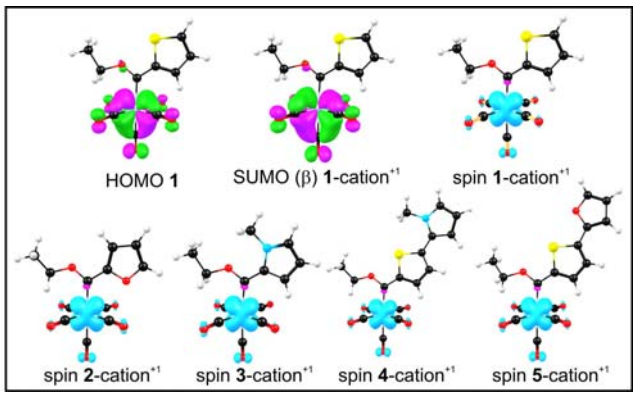

Figure 9: Molecular orbitals related to the first oxidation of 1 - 5: Presentation of (a) the HOMO of the neutral complexes 1, (b) the SUMO of the oxidized (q = +1, s = ½) complexes 1 and (c) the spin density of the oxidized radical cation of complexes 1-5. The MO and spin density plots use a contour of 40 and 4 e/nm^3 respectively. Results were calculated in CH_3CN as solvent.

the SUMO of the oxidized (q = +1, s = ½) **1**, (c) the spin density of the oxidized radical cation of **1-5**. The diagrams for **1-5** clearly show that the first oxidation takes place at the Cr metal centre.

3.3.3 Cr(I)-Cr(II) or Cr(I)-$(CO)_5$Cr(I)=C(OEt)R(+) oxidation?

The second oxidation of **1-5** involves the removal of an electron from the HOMO of the oxidized radical cation of **1-5**. The oxidized radical cation of **1-5** resulted from the removal of a β-electron from the HOMO of the neutral **1-5**. The highest occupied molecular orbital of the oxidized radical cation will thus show where the oxidation will take place; the lowest unoccupied molecular orbital of the doubly oxidized species will give an indication of where the electron had been removed. Evaluation of the relative energies of the molecular orbitals of the oxidized radical cation of **1-5**, showed that the highest occupied molecular orbital is a β-orbital. Removal of a second β-electron, will thus lead to a paramagnetic doubly oxidized species with two unpaired electrons, i.e. with spin = 1. DFT calculations further showed, consistent with the latter, that a doubly oxidized species with spin = 0 was not energetically favoured. The localization of the unpaired free electron of the doubly oxidized species, can be visualized by a spin-density of the oxidized species. Figure 10 shows (a) the β-HOMO of the oxidized radical cation of **1-5**, (b) the β-SUMO of the doubly oxidized (q = +2, s = 1) **1-5** and (c) the spin density of the doubly oxidized **1-5**.

Since the doubly oxidized species is paramagnetic with two unpaired electrons, this second oxidation does not involve the removal of the unpaired spin density (in an α orbital) of the cation of **1-5** shown in Figure 9, as the electron in the β orbital is of higher energy. It therefore involves the removal of this β-electron from the β-HOMO of the cation of **1-5**. In comparing the HOMO of the neutral complex (Figure 9(a), note α-HOMO and β-HOMO are degenerate for neutral complex) with the β-HOMO of the cation of **1-3** (Figure 10(a)), it is clear that, while the first oxidation involved the removal of a d_{xz} electron from the Cr(0) metal centre, the second oxidation involves the removal of a d_{yz} electron from the Cr(I)-metal centre for **1-3**. The distribution of the remaining unpaired electrons after the second oxidation of **1-3** is visualized by the spin density plots in Figure 10(c). The spin has the shape of two

doughnuts on top of each other, typical of two unpaired electrons, one in the d_{xz} and one in the d_{yz} orbital.

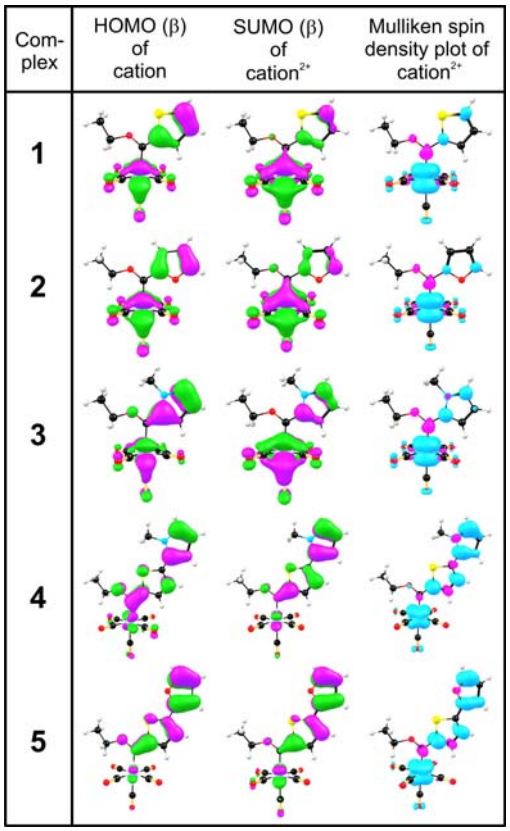

Figure 10: Molecular orbitals related to the second oxidation of 1 - 5: Presentation of (a) the β-HOMO of the oxidized radical cation of 1-5, (b) the β-SUMO of the doubly oxidized (q = +2, s = 1) complexes 1 – 5 and (c) the spin density of the doubly oxidized complexes 1-5. The MO and spin density plots use a contour of 40 and 4 e/nm^3 respectively.

The second oxidation observed for compound **4** at E_{pa} = 0.648 V, occurs at a slightly more positive potential than the first oxidation (0.558 V), and is at a much lower potential than that of compounds **1**−**3** and **5**, see Figure 4. The LSV (not shown) of **4** is consistent with two one electron oxidation processes at E_{pa} = 0.558 and 0.648 V. The DFT calculated adiabatic ionization potential for the removal of the second electron from ($IP_{2e\text{-}}$) for **4** (-6.03 eV) is smaller than for **1** (-7.11 eV), **2** (-7.02 eV), **3** (-6.83 eV) or **5** (-6.36 eV), consistent with the experimental observation that the second oxidation process for **4** occurs at a lower potential. The experimental order of

the second oxidation observed is **4** (0.648 V) < **5** (1.056 V) < **3** (1.132 V) < **2** (1.148 V) < **1** (1.229 V).

Evaluation of the HOMO of the cation of **4** and **5**, indicate that the second oxidation process observed for **4** and **5**, mainly involves the removal of an electron from the dimeric heteroarene five-membered rings, 2,2'-thienylfuran and N-methyl-2-(2'-thienyl)pyrrole) for **4** and **5** respectively, implying that the second oxidation of **4** and **5** leads to a Cr(I)-$(CO)_5$Cr(I)=C(OEt)R(+) radical species. The spin plot in Figure 10(c) showing the distribution of the remaining unpaired electrons after the second oxidation of **4** and **5** is in agreement with this; there is mainly one d_{xz} unpaired electron on the Cr metal centre, the remaining unpaired electron density is distributed over the 2,2'-thienylfuran or N-methyl-2-(2'-thienyl)pyrrole) ligand. It is, however, not clear why the second experimental oxidation of **4** occurs at a potential more than 0.4 V lower than the second oxidation observed for of **1-3** or **5**.

3.3.4 Third oxidation

For **3** - **5** a third experimental oxidation is observed in the same order than the second oxidation: **4** (1.134 V) < **5** (1.158V) < **3** (1.268 V), see Figure 4. The HOMO of **3**-cation^{+2} shows that the third oxidation of **3** involves the oxidation of the 2-(N-methylpyrrolyl)-ring. DFT results show that **3**-cation^{+3} is paramagnetic with three unpaired electrons (S = 3/2), two on Cr and one on the 2-(N-methylpyrrolyl)-ring, see Figure 11. The third oxidation process observed for **4** and **5** is proposed to be metal

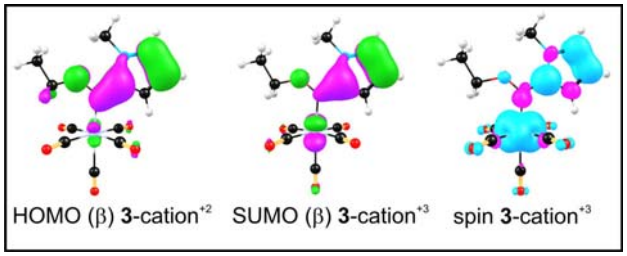

Figure 11: Molecular orbitals related to the third oxidation observed for 3: Presentation of (a) the β-HOMO of 3-cation^{+2}, (b) the β-SUMO of 3-cation^{+3}, (q = +3, s = 3/2) and (c) the spin density of 3-cation^{+3}. The MO and spin density plots use a contour of 40 and 4 e/nm^3 respectively. Results were calculated in CH_3CN as solvent.

based. The spin density plot of **4**-cation^{+3}, shows two unpaired electrons on Cr and another unpaired electron of opposite spin on the N-methyl-2-(2'-thienyl)pyrrole), S = 1/2. For **5**-cation^{+3}, the S = ½ and S = 3/2 states are almost equi-energetic. Both states involve 2 electrons on Cr and one on the ligand.

3.3.5 Electrochemical reduction and DFT energies

The DFT calculated redox properties of complexes **1-5** as determined by the features of the frontier orbitals, viz. HOMO and LUMO energies, adiabatic ionization potential and adiabatic electron affinity, are summarized in Table 3. To take the solvent influence on the electronic structure into account, values for gas phase (ε=1) as well as dichloromethane (DCM, ε=8.9) and acetonitrile (CH_3CN, ε=37.5, the experimental solvent) are reported. The cathodic peak potential (E_{pc}) of the reduction process of **1-5** of this study varies over 0.500 V from -1.47 to -2.00 V *vs*. Fc/Fc$^+$ while the anodic peak potential (E_{pa}) of the first oxidation process of **1-5** lays within a narrow range of 0.070 V from 0.43 to 0.50 V *vs*. Fc/Fc$^+$. The R group in $[(CO)_5Cr{=}C(OEt)R]$ seems to play a significant role in the shape and distribution of electron density of the LUMO orbital of the neutral species, while the HOMO is Cr-based. This suggests that the reduction potential is sensitive to the electrophilic nature of the R substituent, while the oxidation process, that is Cr-based, is relatively insensitive to it. While the character of the LUMO of neutral **1-5** indicates where the reduction will take place, the energy of the LUMO is related to the ease of the reduction. The following linear relationship is obtained between the calculated LUMO energy (in eV) of neutral **1-5** and the formal reduction electrode potential $E^{0'}$ (in V), see Figure 12(a):

$E_{LUMO} = -1.26\ E^{0'}(C_{carbene}) - 4.69$ $(R^2 = 0.98)$ gas phase

$E_{LUMO} = -1.39\ E^{0'}(C_{carbene}) - 4.80$ $(R^2 = 1.00)$ DCM

$E_{LUMO} = -1.41\ E^{0'}(C_{carbene}) - 4.84$ $(R^2 = 1.00)$ CH_3CN

The calculated adiabatic electron affinity EA (in eV), obtained from the energy difference between the neutral and reduced species, is related to formal reduction electrode potential $E^{0'}$ (in V) by (see Figure 12 (b)):

$EA = -1.56\ E^{0'}(C_{carbene}) - 4.02$ $(R^2 = 1.00)$ gas phase

$EA = -1.46\ E^{0'}(C_{carbene}) - 5.16$ $(R^2 = 0.99)$ CH_3CN

$EA = -1.45\ E^{0'}(C_{carbene}) - 5.30$ $(R^2 = 0.99)$ DCM

The accuracy of the relationships above did not change significantly when comparing the results obtained in gas phase, relative to calculations obtained when taking a solvent into account. The results tabulated in Table 3, show that with increased solvent polarity, the calculated electron affinity increases (more positive) and the ionization potential becomes less negative. The excellent relationships obtained between the DFT calculated energies and $E^{0'}(C_{carbene})$ emphasize the role of the R group in the reduction process of $[(CO)_5Cr{=}C(OEt)R]$ complexes. The relationships obtained enables prediction of the reduction potential of a $[(CO)_5Cr{=}C(OEt)R]$ type complex by DFT calculations, before synthesizing it. As a result, the reduction potential can be tuned by replacing different R substituents on the carbene ligand.

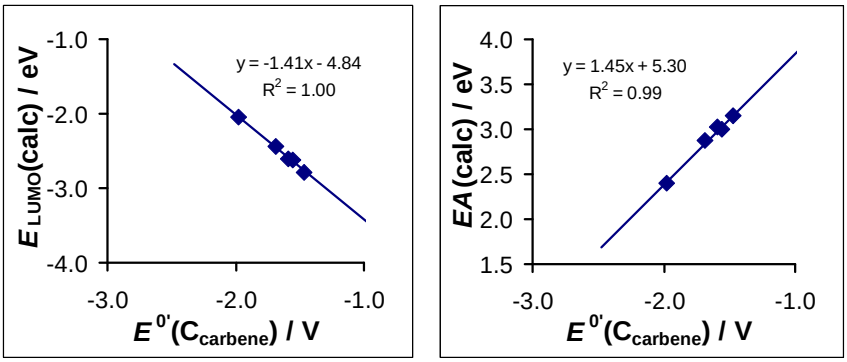

(a) (b)

Figure 12: Linear relationship between the DFT calculated values in CH_3CN as solvent (a) E_{LUMO} and (b) EA of complexes 1-5 and the experimental formal reduction potential $E^{0'}$. Data are in Table 3. Experimental potentials are relative to the Fc/Fc^+ couple.

3.3.6 Electrochemical oxidation and DFT energies

It is already observed that the oxidation process, which is Cr-based, is relatively insensitive to the electrophilic nature of the R substituent of $[(CO)_5Cr{=}C(OEt)R]$ complexes **1-5**. In comparing the HOMO energy of neutral **1-5** with the formal reduction potential of the oxidation process, $E^{0'}$(Cr) of **1-5**, we observe that, while $E^{0'}$(Cr) values of **1-3** relate to the HOMO energy, $E^{0'}$(Cr) values of **4** and **5** are similar to the $E^{0'}$(Cr) of **1,** see Figure 13(a). The failure of the HOMO energies of **4** and **5** to fall on the correlation line may reflect delocalization of the redox active MO of **4** and **5** onto the appended thienyl rings as suggested by the HOMO plots of **4** and **5**, or implies that $E^{0'}$(Cr) of **4** and **5** are insensitive to the influence of the second ring of the dimeric heteroarene five-membered rings in 2,2'-thienylfuran and N-methyl-2-(2'-thienyl)pyrrole). A similar result is obtained when comparing $E^{0'}$(Cr), of **1-5**, with the DFT calculated adiabatic ionization potential, *IP*, of **1-5**, see Figure 13(b).

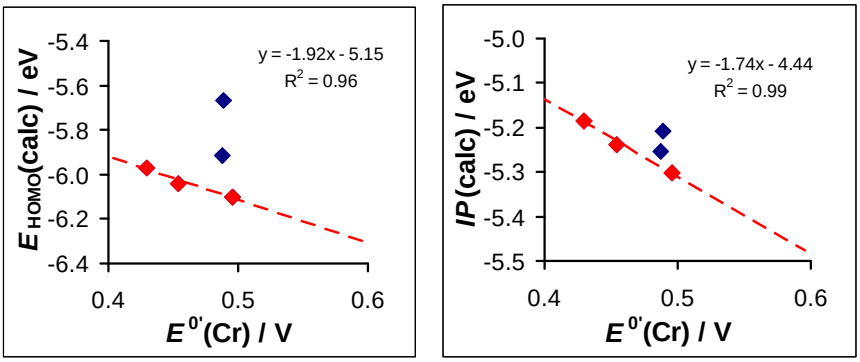

(a) (b)

Figure 13: Linear relationship between the DFT calculated values in CH_3CN as solvent (a) E_{HOMO} and (b) IP of $(CO)_5Cr{=}C(OEt)R$ complexes 1-5 and the experimental formal reduction potential $E^{0'}$(Cr) of the oxidation process of 1-5. Data of complexes 1-3 is indicated in red, and data of 4 and 5 in blue. Data are in Table 3. Experimental potentials are relative to the Fc/Fc^+ couple.

In comparing the empirical relationships obtained, expressed in terms of the redox potentials, we observe relationships that involving $E^{0'}(Cr^{0/I})$ has a much smaller slope relative to relationships involving the reduction potential $E_{pc}(C_{carbene})$:

$E^{0'}(C_{carbene}) = -0.70\ E_{LUMO} - 3.44 = 0.68\ EA - 3.62$ ($R^2 > 0.99$)

$E^{0'}(Cr^{0/I}) = -0.50\ E_{HOMO} - 2.56 = -0.57\ IP - 2.51$ ($R^2 > 0.96$)

The much smaller slope of the relationships reflects the diminished electronic communication between the oxidation centre and the R substituent in $[(CO)_5Cr=C(OEt)R]$ relative to that between the reduction centre and the R.

The empirical relationships obtained here can only be applied to structurally related complexes. It is also possible to calculate adiabatic redox potentials using density functional theory calculations, within an accuracy of ca. 95 - 150 mV [48,49].

4 Conclusions

The R group in $[(CO)_5Cr=C(OEt)R]$ plays a significant role in the energy, shape and distribution of the LUMO orbital, in other words, to the extent of electron delocalization, while the HOMO is Cr-based. Consequently the reduction of $[(CO)_5Cr=C(OEt)R]$ is sensitive to the electrophilic nature of the R substituent, and the cathodic peak potential (E_{pc}) of the reduction process of **1-5** varies over a wide range from -1.49 to -2.01 V *vs*. Fc/Fc^+.

The anodic peak potential (E_{pa}) of the first oxidation process of **1-5** lies within a narrow range of 0.070 V from 0.43 to 0.50 V *vs*. Fc/Fc^+, is Cr-based and is only sensitive to the electrophilic character of the heteroarene ring directly attached to the carbene carbon.

Acknowledgements

This work has received support from the Norwegian Supercomputing Program (NOTUR) through a grant of computer time (Grant No. NN4654K) (JC), the South African National Research Foundation (JC) and the Central Research Fund of the University of the Free State, Bloemfontein (JC) and the University of Pretoria (ML and PHvR). The authors thank Prof. Simon Lotz for providing some of the samples.

Supporting Information

Cif files containing the crystallographic data for this paper, optimized coordinates of the DFT calculations, are available with the on-line version only.

Table 3: Cyclic voltammetry and density functional theory calculated data data for complexes 1–5. Cyclic voltammograms are obtained from 0.0005 mol dm^{-3} solutions of 1–5 in CH_3CN containing 0.1 mol dm^{-3} [^{n}(Bu_4)N][PF_6] as supporting electrolyte on a glassy carbon-working electrode at a scan rate of 0.100 V s^{-1} and 20°C. Experimental potentials are relative to the Fc/Fc$^+$ couple.

Complex	Experimental										Calculated (gas, DCM, CH_3CN)[b]			
	1st reduction				1st oxidation				2nd oxidation	3rd oxidation	neutral complex		anion	cation
	E_{pc}	E_{pa}	$E^{0'}$	ΔE	E_{pa}	E_{pc}	$E^{0'}$	ΔE	E_{pa}	E_{pa}	E_{HOMO} (eV)	E_{LUMO} (eV)	EA (eV)	IP (eV)
1	-1.625	-1.552[a]	-1.589[a,c]	0.073[a]	0.538	0.453	0.496[c]	0.085	1.229	-	-6.097,	-2.738,	1.535,	-6.924,
											-6.099,	-2.620,	2.883,	-5.450,
											-6.100	-2.606	3.021	-5.301
2	-1.719	-1.649[a]	-1.684[a,c]	0.070[a]	0.494	0.414	0.454[c]	0.080	1.148	-	-5.984,	-2.566,	1.354,	-6.820,
											-6.031,	-2.459,	2.732,	-5.381,
											-6.040	-2.444	2.871	-5.239
3	-2.019	-1.938[a]	-1.979[a]	0.081[a]	0.463	0.396	0.430	0.067	1.132	1.268	-5.854,	-2.189,	0.931,	-6.700,
											-5.943,	-2.068,	2.264,	-5.320,
											-5.969	-2.053	2.403	-5.184
4	-1.594	-1.514	-1.554	0.080	0.558	0.420	0.489	0.138	0.648	1.134	-5.735,	-2.674,	1.592,	-6.615,
											-5.673,	-2.623,	2.861,	-5.393,
											-5.668	-2.622	2.998	-5.201
5	-1.494	-1.435	-1.468	0.066	0.531	0.444	0.488	0.087	1.056	1.158	-5.926,	-2.841,	1.728,	-6.703,
											-5.916,	-2.787,	3.007,	-5.388,
											-5.917	-2.786	3.146	-5.255

a Values determined from data of 0.300 V s^{-1} scan.

b Calculated values are given in the order: gas phase value, value calculated in DCM as solvent, value calculated in CH_3CN as solvent.

c $E^{0'}$ = -1.762 and 0.565 (complex 1) and -1.883 and 0.495 (complex 2) in DCM [11].

References

[1] K. H. Dötz, H. Fischer, P. Hofmann, F. R. Kreissl, U. Schubert and K. Weiss, Transition Metal Carbene Complexes, VCH, Verlag, Weinheim, (1983).

[2] M. Landman, H. Görls and S. Lotz, Chromium and Tungsten Carbene Complexes of Thieno[3,2-b]thiophene, European Journal of Inorganic Chemistry (2001) 233.

[3] S. Lotz, M. Landman, H. Görls, C. Crause, H. Nienaber and A. J. Olivier, Di-tungsten Bis-carbene Complexes Linked by Condensed Heteroaromatic Spacers, Zeitschrift für Naturforschung 62b (2007) 419.

[4] J.W. Herndon, Applications of carbene complexes toward organic synthesis, Coordination Chemistry Reviews 206–207 (2000) 237.

[5] C.A. Merlic, Y. You, D.M. McInnes, A.L. Zechman, M.M. Miller, Q. Deng, Benzannulation reactions of Fischer carbene complexes for the synthesis of indolocarbazoles, Tetrahedron, 57 (2001) 5199.

[6] H. Dialer, K. Polborn, W. Beck, Metal complexes of biologically important ligands, Part CXVIII. Metathesis of dehydro amino acids with Fischer carbene complexes: synthesis of complexes of amino acid- and peptide-α-carbenes and of isoindoles, Journal of Organometallic Chemistry 589 (1999) 21.

[7] I. Hoskovcová, J. Roháčová, L. Meca, T. Tobrman, D. Dvořák, J. Ludvík, Electrochemistry of chromium(0)–aminocarbene complexes The use of intramolecular interaction LFER for haracterization of the oxidation and reduction centre of the complex, Electrochimica Acta 50 (2005) 4911.

[8] I. Hoskovcová, J. Roháčová, D. Dvořák, T. Tobrman, S. Záliš, R. Zvěřinová, J. Ludvík, Synthesis and electrochemical study of iron, chromium and tungsten aminocarbenes: Role of ligand structure and central metal nature, Electrochimica Acta 55 (2010) 8341.

[9] I. Hoskovcová, R. Zvěřinová, J. Roháčová, D. Dvořák, T. Tobrman, S. Záliš, J. Ludvík, Fischer aminocarbene complexes of chromium and iron: Anomalous electrochemical reduction of p-carbonyl substituted derivatives, Electrochimica Acta 56 (2011) 6853.

[10] R. Metelková, T. Tobrman, H. Kvapilová, I. Hoskovcová, J. Ludvík, Synthesis, characterization and electrochemical investigation of hetaryl chromium(0) aminocarbene complexes, Electrochimica Acta 82 (2012) 470.

[11] B. van der Westhuizen, P. J. Swarts, L.M. van Jaarsveld, D.C. Liles, U. Siegert, J. C. Swarts, I. Fernández, and D. I. Bezuidenhout, Substituent Effects on the Electrochemical, Spectroscopic, and Structural Properties of Fischer Mono- and Biscarbene Complexes of Chromium(0), Inorg. Chem. 52 (2013) 6674-6684.

[12] M. Landman, J. Ramontja, M. van Staden, D.I. Bezuidenhout, P.H. van Rooyen, D.C. Liles, S. Lotz, Properties of homo- and heteronuclear mixed biscarbene complexes with conjugated bithiophene units, Inorganica Chimica Acta 363 (2010) 705.

[13] D.F. Shriver, M.A. Drezdon, The manipulation of air sensitive compounds, 2nd edition, John Wiley and Sons, New York, (1986).

[14] G.H. Spies, R.J. Angelici, Model Studies of Thiophene Hydrodesulfurization Using (η-Thiophene)Ru(η-C5H5)$^{+}$: Reactions Leading to C-S Bond Cleavage, Organometallics 6 (1987) 1897.

[15] H. Meerwein, Triethyloxonium Fluoborate, Organic Syntheses 46 (1966) 113.
[16] A.J. Olivier, MSc dissertation, Novel carbene complexes with pyrrole ligands, University of Pretoria, (2001).
[17] APEX2 (including SAINT and SADABS); Bruker AXS Inc., Madison, WI, (2013).
[18] G.M. Sheldrick, A short history of SHELX, Acta Crystallographica A 64 (2008) 112.
[19] D.T Sawyer, J.L Roberts (Jr), Experimental Electrochemistry for Chemists, Wiley, New York, (1974) 54.
[20] D.H. Evans, K.M. O'Connell,.R.A. Peterson, M.J. Kelly, Cyclic voltammetry, Journal of Chemical Education 60 (1983) 290.
[21] G.A. Mabbott, An introduction to cyclic voltammetry, Journal of Chemical Education 60 (1983) 697.
[22] G. Gritzner, J. Kuta, Recommendations on reporting electrode potentials in nonaqueous solvents, Pure and Applied Chemistry 56 (1984) 461.
[23] A.J.L. Pombeiro, Electron-donor/acceptor properties of carbynes, carbenes, vinylidenes, allenylidenes and alkynyls as measured by electrochemical ligand parameters, Journal of Organometallic Chemistry 690 (2005) 6021.
[24] A.D. Becke, Density-functional exchange-energy approximation with correct asymptotic behavior, Physical Review A 38, (1988) 3098.
[25] C. Lee, W. Yang, R.G. Parr, Development of the Colle-Salvetti correlation-energy formula into a functional of the electron density, Physical Review B 37 (1988) 785.
[26] Gaussian 09, Revision C.01, M. J. Frisch, G. W. Trucks, H. B. Schlegel, G. E. Scuseria, M. A. Robb, J. R. Cheeseman, G. Scalmani, V. Barone, B. Mennucci, G. A. Petersson, H. Nakatsuji, M. Caricato, X. Li, H. P. Hratchian, A. F. Izmaylov, J. Bloino, G. Zheng, J. L. Sonnenberg, M. Hada, M. Ehara, K. Toyota, R. Fukuda, J. Hasegawa, M. Ishida, T. Nakajima, Y. Honda, O. Kitao, H. Nakai, T. Vreven, J. A. Montgomery, Jr., J. E. Peralta, F. Ogliaro, M. Bearpark, J. J. Heyd, E. Brothers, K. N. Kudin, V. N. Staroverov, T. Keith, R. Kobayashi, J. Normand, K. Raghavachari, A. Rendell, J. C. Burant, S. S. Iyengar, J. Tomasi, M. Cossi, N. Rega, J. M. Millam, M. Klene, J. E. Knox, J. B. Cross, V. Bakken, C. Adamo, J. Jaramillo, R. Gomperts, R. E. Stratmann, O. Yazyev, A. J. Austin, R. Cammi, C. Pomelli, J. W. Ochterski, R. L. Martin, K. Morokuma, V. G. Zakrzewski, G. A. Voth, P. Salvador, J. J. Dannenberg, S. Dapprich, A. D. Daniels, O. Farkas, J. B. Foresman, J. V. Ortiz, J. Cioslowski, and D. J. Fox, Gaussian, Inc., Wallingford CT, (2010).
[27] T.H. Dunning Jr., P.J. Hay, Modern Theoretical Chemistry, Ed. H.F. Schaefer III, Vol. 3 Plenum, New York, (1976) 1.
[28] P.J. Hay, W.R. Wadt, Ab initio effective core potentials for molecular calculations. Potentials for the transition metal atoms Sc to Hg, Journal of Chemical Physics 82 (1985) 270.
[29] P.J. Hay, W.R. Wadt, Ab initio effective core potentials for molecular calculations. Potentials for main group elements Na to Bi, Journal of Chemical Physics 82 (1985) 284.
[30] P.J. Hay, W.R. Wadt, Ab initio effective core potentials for molecular calculations. Potentials for K to Au including the outermost core orbitals, Journal of Chemical Physics 82 (1985) 299.

[31] I.J.S. Fairlamb, Regioselective (site-selective) functionalisation of unsaturated halogenated nitrogen, oxygen and sulfur heterocycles by Pd-catalysed cross-couplings and direct arylation processes, Chemical Society Reviews 36 (2007) 1036.

[32] S.P. Stanforth, Catalytic cross-coupling reactions in biaryl synthesis, Tetrahedron 54 (1998) 263.

[33] T. Tamao, S. Kodama, I. Nakajima, M. Kumada, A.Minto and K.Suzuki, Nickel-phosphine complex-catalyzed Grignard coupling—II : Grignard coupling of heterocyclic compounds, Tetrahedron 38 (1982) 3347.

[34] N. Jayasuriya and J. Kagan, The Synthesis of Bithienyls and Terthienyls by Nickel-catalyzed Coupling of Grignard Reagents, Heterocycles 24 (1986) 2261.

[35] A. Minato, K. Tamao, T. Hayashi, K. Suzuki and M. Kumada, Palladium-phosphine complex catalyzed cross-coupling reaction of 1-methyl-2-pyrrolyl-magnesium bromide and -zinc chloride with organic halides, Tetrahedron Letters 22 (1981) 5319.

[36] G.T. Crisp, Palladium Mediated Formation of Bithiophenes, Synthetic Communications 19 (1989) 307.

[37] L. Brandsma, S. F. Vasilevsky, and H. D. Verkruijsse, Application of Transition Metal Catalysts in Organic Synthesis, Springer-Verlag, Berlin/Heidelberg, (1998).

[38] S. Lotz, C Crause, A.J. Olivier, D.C. Liles, H. Görls, M. Landman, D.I. Bezuidenhout, Synthesis and reactivity of metal carbene complexes with heterobiaryl spacer substituents, Dalton Transactions (2009), 697.

[39] L. Brandsma, S. F. Vasilevsky, and H. D. Verkruijsse, Application of Transition Metal Catalysis in Organic Synthesis, Springer-Verlag, Berlin/Heidelberg (1998) 15.

[40] L. Brandsma, S. F. Vasilevsky, and H. D. Verkruijsse, Application of Transition Metal Catalysis in Organic Synthesis, Springer-Verlag, Berlin/Heidelberg (1998) 264.

[41] D. J. Chadwick and C.Wilbe, High-yield syntheses of dilithio-derivatives of furan, thiophen, N-methylpyrrole, 3-methylfuran, and 3-methylthiophen. Application of the method to 2-methylfuran, 2-methylthiophen, 2,5-dimethylfuran, 2,5-dimethylthiophen, benzo[b]furan, benzo[b]thiophen, pyrrole, and indole, Journal of the Chemical Society, Perkin Transactions 1 (1977) 887.

[42] A. Carpita, R. Rossi and C. A. Veracini, Synthesis and ^{13}C NMR characterization of some π-excessive heteropolyaromatic compounds, Tetrahedron, 41 (1985) 1919.

[43] J.A. Connor, E.M. Jones, Stabilisation of nucleophilic carbenes co-ordinated to transition metals, Journal of the Chemical Society (A) (1971), 1974.

[44] A.B.P. Lever, Electronic characteristics of an extensive series of ruthenium complexes with the non-innocent o-benzoquinonediimine ligand: A pedagogical approach, Coordination Chemistry Reviews 254 (2010) 1397.

[45] W. Kaim, B. Schwederski, Non-innocent ligands in bioinorganic chemistry - An overview, Coordination Chemistry Reviews 254 (2010) 1580.

[46] P. T. Kissinger and W. R. Heineman, Cyclic voltammetry, Journal of Chemical Education 60 (1983) 702.

[47] C.P. Casey, L.D. Albin, M.C. Saeman and D.H. Evans, The electrochemical reduction of arylmethoxycarbene complexes of chromium, molybdenum and tungsten, Journal of Organometallic Chemistry 155 (1978) C37.
[48] M. Baik, R.A. Friesner, Computing Redox Potentials in Solution: Density Functional Theory as A Tool for Rational Design of Redox Agents, Journal of Physical Chemistry 106 (2002) 7407.
[49] H. Vázquez-Lima, P. Guadarrama, Analysis of Structural Factors Related to Spectroscopic Data and Redox Potentials of CuT1 Models Through DFT Tools, International Journal of Quantum Chemistry, 112 (2012) 1431.